1-1-2011

Dispersion of SnO2 nanocrystals on TiO2(B) nanowires as anode material for lithium ion battery applications

Zunxian Yang
Fuzhou University China

Guodong Du
University of Wollongong, gd616@uow.edu.au

Qing Meng
University of Wollongong, qm982@uowmail.edu.au

Zaiping Guo
University of Wollongong, zguo@uow.edu.au

Xuebin Yu
xyu@uow.edu.au

See next page for additional authors

RSC Advances

Cite this: *RSC Advances*, 2011, **1**, 1834–1840

www.rsc.org/advances

PAPER

Dispersion of SnO_2 nanocrystals on TiO_2(B) nanowires as anode material for lithium ion battery applications†

Zunxian Yang,*[a] Guodong Du,[b] Qing Meng,[bc] Zaiping Guo,*[bc] Xuebin Yu,*[d] Zhixin Chen,[c] Tailiang Guo[a] and Rong Zeng[b]

Received 22nd July 2011, Accepted 13th September 2011
DOI: 10.1039/c1ra00500f

TiO_2(B)@SnO_2 core–shell hybrid nanowires have been synthesized by a facile hydrothermal process and subsequent liquid phase reaction. Hybrid nanowire electrodes exhibit excellent reversible lithium storage capacity rate capability and good cyclability, mainly due to the particular architecture of the composite, which features an open continuous channel along its axis, facilitating lithium ion diffusion, and provides effective mechanical support for the TiO_2(B) core, alleviating the stress produced during discharge–charge cycling and also preventing the pulverization of the Sn nanoparticles. Owing to its superior electrochemical performance, this composite could be a promising potential anode material for lithium ion batteries.

Introduction

SnO_2 nanomaterials have received considerable attention for their myriad of applications in gas sensors,[1–7] photocatalysis[8] and lithium ion batteries,[9–11] owing to their attractive electronic, optical, and electrochemical properties. To date, various one-dimensional SnO_2 nanostructures, in such forms as nanorods/arrays,[12–14] nanobelts,[15,16] nanowires,[2,3,17] and nanotubes,[18–19] have been prepared by many synthesis methods, including thermal evaporation,[5,20] chemical vapor deposition,[1] the hydrothermal method,[12] the template method,[3,21] *etc.* As one of the most promising anode materials for lithium ion batteries, one-dimensional (1D) SnO_2 nanomaterials have attracted particular attention because of their high capacity compared with that of graphite (372 mA h g^{-1}).[22,23] Nevertheless, practical implementation of 1D SnO_2 nanomaterials in lithium-ion batteries is greatly frustrated by the large initial irreversible capacity induced by Li_2O formation and the abrupt capacity fading caused by volume variation (up to 258%[24]).

Using core–shell composite architectures may be one of most effective strategies to improve the Li^+ storage capacity and cyclability of one-dimensional SnO_2-based nanomaterials because of the "buffering" and "mechanical support" functions[25,26] of the core materials during charge–discharge cycling. Presently, various core–shell 1D SnO_2-based composites, such as carbon/SnO_2,[27] MgO/SnO_2,[28] TiO_2/SnO_2,[29] *etc.*, have been prepared and have exhibited excellent optoelectronic performance, which enables the potential application of those materials in lithium ion batteries. However, up to now, only a few core–shell SnO_2 based composites besides carbon/SnO_2 have been explored for anode material applications in lithium ion batteries, probably because of their complicated chemical and physical synthesis processes. Thus, there are still many challenges in synthesizing one-dimensional TiO_2@SnO_2 hybrid nanomaterials by facile synthesis routes. TiO_2(B) is a metastable monoclinic modification of titanium dioxide. It has been demonstrated that the kinetics of lithium storage in TiO_2(B) are governed by a pseudo-capacitive Faradaic process, which is not limited by solid-state diffusion of Li ions.[30] TiO_2(B) has an open structure with freely accessible channels for Li ion transport perpendicular to the (010) face, which allows easy Li^+ transport.

Herein, we report TiO_2(B)@SnO_2 hybrid nanowires, each consisting of a TiO_2(B) nanowire core covered with a SnO_2 nanocrystal shell, which are simply prepared by a hydrothermal reaction between NaOH and TiO_2 powder, followed by a liquid phase reaction process in $SnCl_2 \cdot 2H_2O$ and urea solution, and finally by dehydrating and drying in an oven. These TiO_2(B)@SnO_2 hybrid nanowires exhibit excellent lithium storage capacity and good cyclability, revealing their potential for application in lithium ion batteries.

Experimental

Synthesis of TiO_2(B)@SnO_2 hybrid nanowires

TiO_2(B)@SnO_2 hybrid nanowires were fabricated *via* a facile hydrothermal process and subsequent liquid phase reaction.

[a]*Engineering Research Center for Field Emission Display Technology of the Ministry of Education, Fuzhou University, Fuzhou, 350002, P. R. China*
[b]*Institute for Superconducting & Electronic Materials, University of Wollongong, NSW, 2522, Australia*
[c]*School of Mechanical, Materials & Mechatronics Engineering, University of Wollongong, NSW, 2522, Australia*
[d]*Department of Materials Science, Fudan University, Shanghai, 200433, P. R. China. E-mail: zguo@uow.edu.au; yangzunxian@hotmail.com; yuxuebin@fudan.edu.cn; Fax: +61 2 4221 5731; Tel: +61 2 4221 5225*
† Electronic Supplementary Information (ESI) available. See DOI: 10.1039/c1ra00500f/

Typically, the precursors, titanate nanowires, were synthesized by adding 4.5 g TiO_2-anatase (99.8%, Aldrich) to a 22 ml 15 M aqueous solution of NaOH. After stirring for 1 h, the resulting suspension was transferred to a 30 ml Teflon-lined autoclave and heated at 150 °C for 72 h. The product was acid washed, which involved stirring the sample in 0.1 M HCl solution for 1 h, twice, resulting in the parent $H_2Ti_3O_7$ nanowires.[31–34] The material was then filtered, repeatedly washed with distilled water until pH ≈ 7, and dried at 80 °C for 20 h. Subsequently, the as-prepared materials were heated at 400 °C for 4 h in air. Then, 0.3 g as-prepared powder was dispersed into 20 ml de-ionized (DI) water to obtain a white suspension by ultrasonication and subsequent stirring. The suspension was subjected to a 60 °C water bath with continuous stirring. Then, 0.162 ml 37% hydrochloric acid was dropped into the suspension. After this process, based on many preliminary experiments, 0.67 g $SnCl_2{\cdot}2H_2O$ and 0.33 g urea were added in sequence. In the process above, the urea functions as the precipitant, owing to the slow hydrothermal reaction at this temperature. This thermostatic reaction lasted about 20 min with continuous stirring. The final product was obtained by washing with DI water, filtering, and drying.

Materials characterization

The morphology of the TiO_2(B)@SnO_2 nanowires was evaluated using a JEOL 7500FA field emission scanning electron microscope (FE-SEM, JEOL, Tokyo, Japan) and a JEOL 2011F transmission electron microscope (TEM, JEOL, Tokyo, Japan). The crystal structures of the TiO_2(B)@SnO_2 nanowires were obtained using X-ray diffraction (XRD) data (MMA, GBC, Australia). Energy dispersive X-ray spectroscopy (EDX, JEOL 7500FA) was used to confirm the concentrations of TiO_2 and SnO_2. X-Ray photoelectron spectroscopy (XPS) experiments were carried out on a VG Scientific ESCALAB 220IXL instrument using aluminum Kα X-ray radiation during XPS analysis.

Electrochemical characterization

Electrochemical properties were measured on electrodes prepared by compressing a mixture of as-prepared TiO_2(B)@SnO_2 hybrid nanowires, carbon black (Super P, MMM, Belgium), and poly(vinyl difluoride) (PVDF) binder in a weight ratio of 70 : 15 : 15 and pasting the mixture on copper foil. Pure lithium metal foil was used for the counter and reference electrodes. The electrolyte was $LiPF_6$ (1 M) in a mixture of ethylene carbonate (EC) and dimethyl carbonate (DMC) (1 : 1 v/v; MERCK KgaA, Germany). Coin cells were assembled in a high-purity argon-filled glove box (Mbraun, Unilab, Germany). A LAND-CT2001A instrument was used with a charge-discharge current density of 30 mA g^{-1} to measure the electrochemical capacity of the electrodes at room temperature by the galvanostatic method. Rate capability tests of the electrodes were then carried out systematically. The cut-off potentials for charge and discharge were set at 3.0 and 0.01 V *versus* Li^+/Li, respectively. To explore the contribution of the TiO_2 in the composite to the capacity of the electrodes, the cycling performance of the electrodes was also evaluated with cut-off potentials of 3.0 and 1.0 V *versus* Li^+/Li, respectively. Cyclic voltammetry (CV) was performed on a PARSTAT@2273 electrochemical workstation.

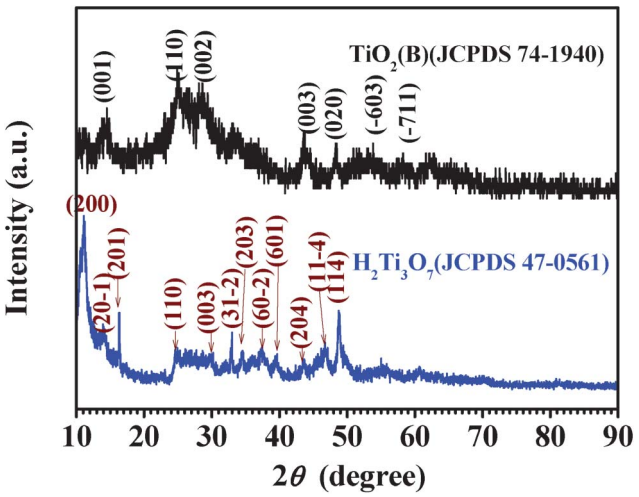

Fig. 1 X-Ray diffraction patterns of as-prepared $H_2Ti_3O_7$ nanowires and TiO_2(B)@SnO_2 nanowires.

Results and discussion

As shown in Fig. 1, X-ray diffraction (XRD) analysis of the as-synthesized parent titanate nanowires and TiO_2@SnO_2 hybrid nanowires reveals that the parent titanate nanowires are $H_2Ti_3O_7$[31–34] with monoclinic structure (JCPDS 47-0561) and undergo consecutive phase transitions to TiO_2(B) (JCPDS 74-1940), with the final stage consisting of TiO_2@SnO_2 hybrid nanowires, after hydrothermal processing and the subsequent liquid phase reaction. There are no sharp characteristic peaks in the X-ray diffraction pattern, possibly because of the poor crystallinity of the titanate just after the hydrothermal process, as well as the interference of a thick, nanocrystalline or amorphous SnO_2 particle layer on the surface of the hybrid nanowires. Furthermore, TiO_2(B) is the main phase of the TiO_2@SnO_2 hybrid nanowires, belonging to space group *C*2/*m* (12) with lattice parameters of a = 12.1787 Å, b = 3.7412 Å, c = 6.5249 Å, and β = 107.054°, while $H_2Ti_3O_7$ is the main phase of the parent titanate nanowires. Additionally, no obvious characteristic peak of SnO_2 has been detected, which is due to the nanocrystalline or amorphous nature of the SnO_2 in the composite. The as-synthesized nanowires display a homogenous, one-dimensional morphology, as shown in the field-emission scanning electron microscope (FE-SEM) images (Fig. 2 and ESI,† Fig. S1). The $H_2Ti_3O_7$ nanowires have diameters of 30–120 nm and extend to a few micrometres in length (Fig. 2(a–b) and ESI,† Fig. S1(a,b)). In order to reduce the electrostatic charging during the FE-SEM imaging of the $H_2Ti_3O_7$ sample, gold nanoparticles were evaporated on it and can clearly be seen in Fig. 2(b) and Fig. S1(b).† After heat-treatment and the subsequent liquid phase reaction process, as shown in Fig. 2(c,d) and Fig. S1(c,d),† these TiO_2(B)@SnO_2 hybrid nanowires become slightly thicker than the $H_2Ti_3O_7$ precursor nanowires, mainly due to the encapsulation of the TiO_2 nanowires by a thick layer of porous SnO_2 nanoparticles (see Fig. 2(d)), which, to some extent, facilitate lithium ion storage and Li^+ diffusion due to the high specific surface area and high porosity. More interestingly, some TiO_2(B)@SnO_2 hybrid nanowires have aggregated to form a three-dimensional (3D) microstructure. There are also many

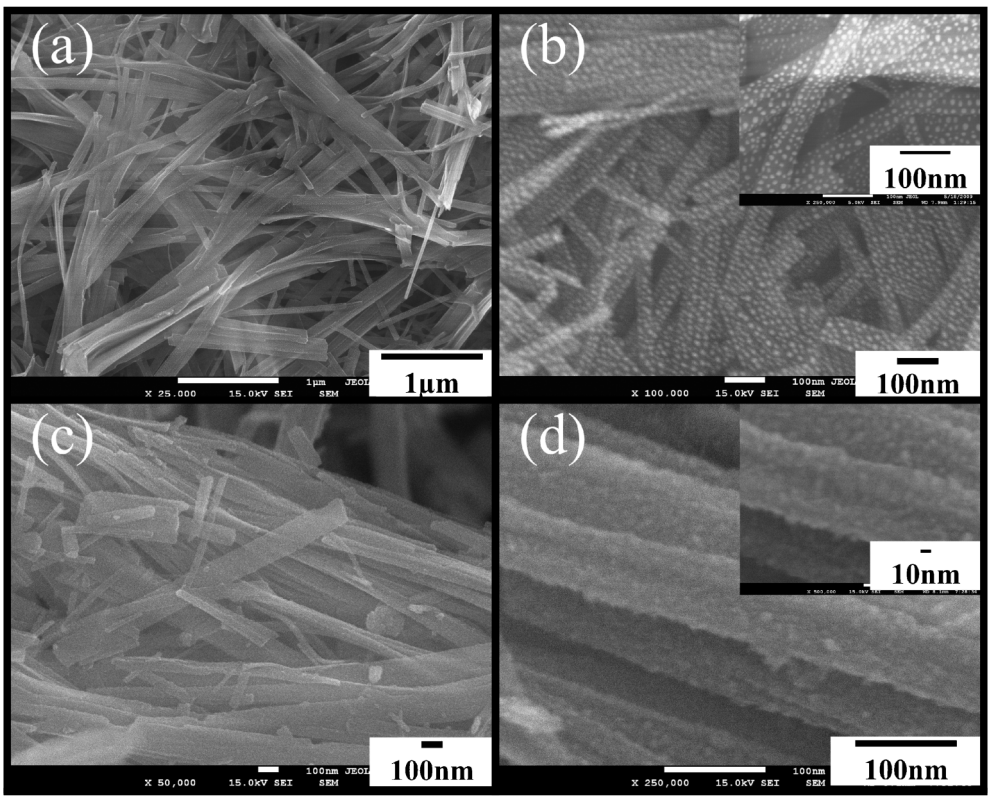

Fig. 2 FE-SEM images of as-synthesized $H_2Ti_3O_7$ nanowires and TiO_2(B)@SnO_2 nanowires: (a) $H_2Ti_3O_7$ nanowires, (b) $H_2Ti_3O_7$ nanowires at high magnification and at higher magnification (inset), (c) TiO_2(B)@SnO_2 nanowires, (d) close-up of a few TiO_2(B)@SnO_2 nanowires with porous surface structure, with inset showing details. (Gold nanoparticles with grain sizes of ~5–10 nm were evaporated on the surface of the $H_2Ti_3O_7$ nanowire samples to reduce electrostatic charging during SEM imaging.)

mesopores or gaps formed by these 3D microstructures in the electrode material, which favor electrolyte diffusion.

Transmission electron microscope (TEM) images combined with selected-area electron diffraction (SAED) patterns reveal the fine microstructure of the parent $H_2Ti_3O_7$ nanowires and the TiO_2(B)@SnO_2 hybrid nanowires, respectively (Fig. 3 and Fig. S2(a,b)†). Fig. 3(a) shows the TEM image and SAED pattern (inset) of a single $H_2Ti_3O_7$ nanowire. Each $H_2Ti_3O_7$ nanowire is actually a monocrystal with monoclinic structure extending along the [200]* direction (Fig. 3(a) and its inset), which is similar to the results of Peng's group.[35,36] Fig. 3(b) shows a TEM image and SAED pattern (inset) of random $H_2Ti_3O_7$ nanowires. Due to the random orientation of these nanowires, the two most intensive diffraction rings were indexed as the (200) and (003) planes of $H_2Ti_3O_7$ (see Fig. 3(b) and its inset). As shown in Fig. 3(c), a TiO_2(B)@SnO_2 nanowire, inheriting the monoclinic structure characteristics of a $H_2Ti_3O_7$ nanowire, extends along the $[010]_B$* direction, according to the SAED pattern of a single hybrid nanowire (Fig. 3(c) inset). Similarly, due to the random orientation of the hybrid nanowires, the two most intensive diffraction rings were indexed as the (002) and (110) planes of TiO_2(B) (see Fig. 3(d) and its inset). Additionally, it can be observed that SnO_2 nanoparticles are decorated on the surface of the TiO_2(B) nanowire core (Fig. 3(c,d) and Fig. S2(a,b)†), according to the obvious fringes of the SnO_2 nanocrystals in the high resolution TEM (HRTEM) image (Fig. S2(b)†). However, it is difficult to distinguish the SnO_2 phase in the composite from the SAED patterns, which may be attributable to the nanocrystalline nature of the SnO_2 nanoparticles in the composite. Thus, both HRTEM and SAED investigations confirm the presence of single-crystalline TiO_2(B) and SnO_2 nanocrystals. This SnO_2 nanocrystal layer forms an effective core–shell 1D structure in conjunction with the TiO_2(B) nanowire itself. It has been reported that TiO_2(B) nanowires extending along the [010] direction[31–34] are characterized by continuous, freely accessible, parallel channels which will enhance Li^+ diffusion. Therefore, in the hybrid nanowires, the TiO_2(B) core could provide continuous channels favorable to Li^+ diffusion along the length axis of the nanowire, in addition to its mechanical support function for the ~30% (wt%) of porous SnO_2 nanocrystals (Fig. S2(c)†). This supporting function of the TiO_2(B) core to some extent helps to alleviate the stress caused during lithium intercalation/de-intercalation.

X-Ray photoelectron spectroscopy (XPS) analysis of the TiO_2(B)/SnO_2 hybrid nanowires was performed from 0 to 1100 eV (Fig. 4). The Ti2p spectrum (Fig. 4(a)) for TiO_2(B)/SnO_2 comprises two symmetrical peaks with binding energies (BEs) of 458.89 eV and 464.61 eV, which are attributable to Ti2p3/2 and Ti2p1/2, respectively. The separation between these two peaks is 5.72 eV, slightly larger than the energy splitting reported for TiO_2.[37,38] This is possibly because of the encapsulation of TiO_2(B) in SnO_2 nanocrystals. Similarly, there are two symmetrical peaks with BEs at 487.20 eV and 495.46 eV in the Sn3d spectrum (Fig. 4(b)) of TiO_2(B)@SnO_2, which are derived

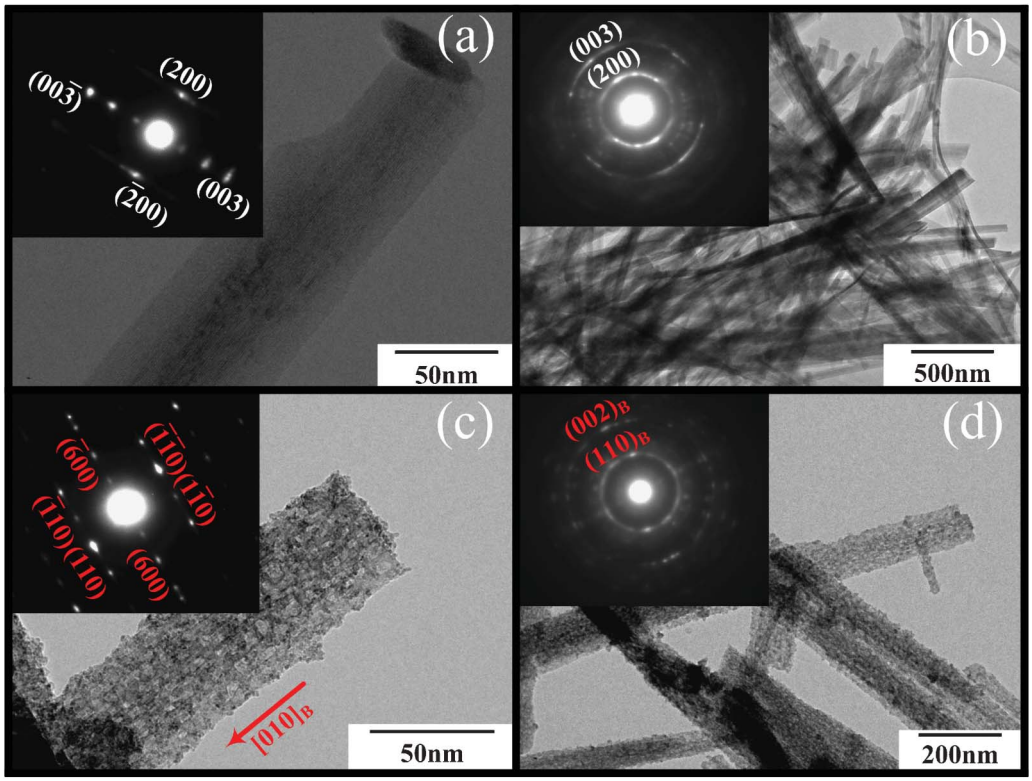

Fig. 3 (a) TEM image and SAED pattern (inset) of single $H_2Ti_3O_7$ nanowire, (b) low-magnification TEM image and SAED pattern (inset) of $H_2Ti_3O_7$ nanowires, (c) TEM image and SAED pattern (inset) of single TiO_2(B)@SnO_2 nanowire, (d) low-magnification TEM image and SAED pattern (inset) of $H_2Ti_3O_7$ nanowires. (In these TEM patterns, subscript 'B' represents the 'TiO_2(B)'.)

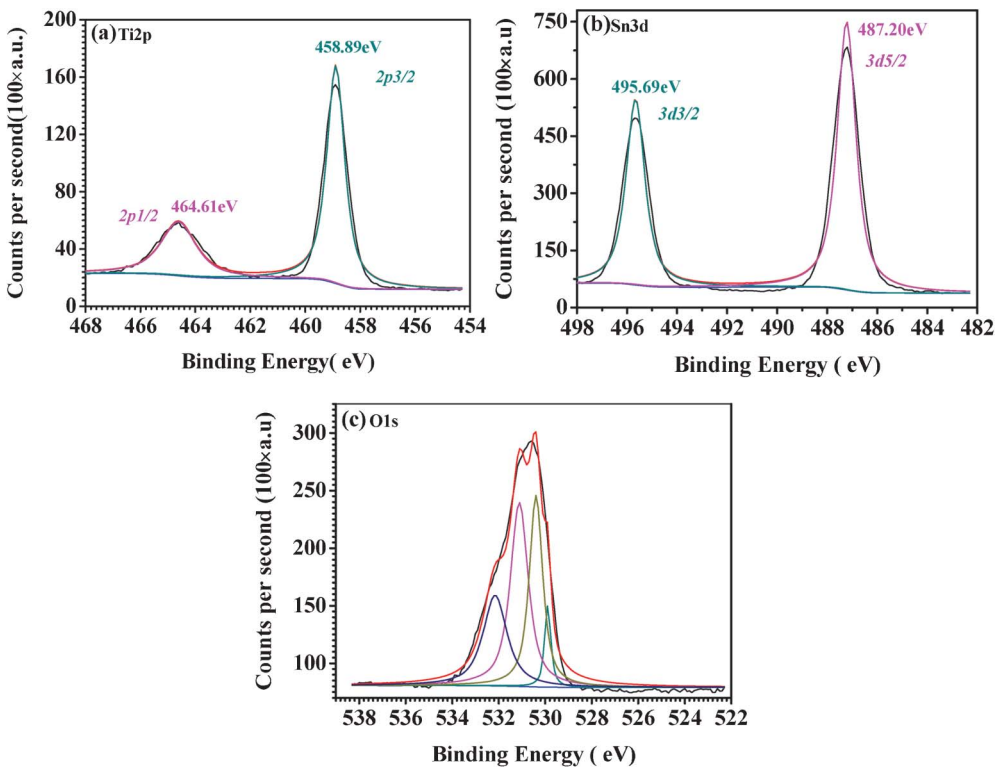

Fig. 4 XPS high-resolution spectra of the (a) Ti2p, (b) Sn3d, and (c) O1s regions for the as-prepared TiO_2(B)@SnO_2 nanowires.

from Sn3d5/2 and Sn3d3/2, respectively. The separation between them, equal to 8.26 eV, is in good agreement with the energy splitting reported for SnO_2.[39–41] As for the O1s spectrum shown in Fig. 4(c), a portion could come from TiO_2, as evidenced by the O1s BE peak at ~529.90 eV,[42] while the peak at 530.40 eV may be due to the SnO_2 in the composite. Additionally, there are two higher O1s BE peaks at 531.10 eV and 532.187 eV, which possibly originate from the OH^- radical, adsorbed oxygen, or adsorbed H_2O.[37,42] These results combined with the XRD, FE-SEM, TEM, and XPS results, confirm that the as-synthesized TiO_2(B)/SnO_2 hybrid nanowire composites have a TiO_2(B) crystal core inside a shell of porous SnO_2 nanocrystals. In addition, some pores or gaps are formed by bundling of the nanowires (Fig. S1†) in the sample, all of which would favor the enhancement of the electrochemical performance of the electrode, due to their contribution in terms of accommodating the electrolyte and favoring lithium ion diffusion during the charge–discharge process.

The electrochemical performance of the TiO_2(B)/SnO_2 hybrid nanowire electrode was subsequently investigated as an anode material for lithium ion batteries. Fig. 5(a) shows cyclic voltammograms (CVs) of the TiO_2/SnO_2 hybrid nanowires from the first to the fifth cycle at a scan rate of 0.1 mV s^{-1} in the voltage range 0.0–3.0 V. The curve of the initial cycle is different from later ones, especially with respect to the subsequent gradual disappearance of some high voltage CV peaks, possibly owing to the formation of an inactive solid–electrolyte interface (SEI) on the surface of the active material, which is inclined to intercept reversible Li ion pathways into/out of the TiO_2(B) core in the discharge–charge process.[43] In the first cycle, the cathodic/anodic peak pairs at 0.012 V, 0.175 V, 0.437 V, and 0.584 V are mainly related to the formation of various Li_xSn phases such as Li_2Sn_5, LiSn, Li_7Sn_3, Li_5Sn_2, $Li_{13}Sn_5$, Li_7Sn_2, and $Li_{22}Sn_5$ during the charge–discharge process,[11] while the small cathodic/anodic peak pair at around 0.968 V and 1.265 V is possibly derived from Li_2O formation and electrolyte decomposition,[44] which causes a large irreversible capacity in the first few cycles that gradually disappears in the subsequent cycles, as shown in Fig. 5(a). There remains two obvious cathodic/anodic peak pairs at 1.45 V and 1.583 V, and 1.51 V and 1.663 V in the first cycle, while the two cathodic peaks change to and stabilize at 1.483 V and 1.551 V, respectively, in the subsequent cycles, which is probably attributable to lithium ion insertion into/extraction out of TiO_2(B).[30,45] Another small cathodic/anodic peak pair at 1.716 V and 1.95 V corresponds to the reaction of Li^+ with a trace amount of anatase[46] in the composite. After the first CV cycle, the electrode demonstrates quite reversible behavior in terms of the reaction, according to Fig. 5(a). It is apparent that the TiO_2 core provides a supporting function which alleviates the pulverization and drastic volume variation of the SnO_2. There may also be the formation of an electrochemically-active Sn/Sn-Ti-O bilayer[43] in the TiO_2@SnO_2 hybrid nanowire, which functions as a stable molecular membrane for Li-ion insertion and extraction processes, and will thus facilitate reversible Li-ion behavior.

The discharge–charge cycling performance was evaluated between 3 V and 0.01 V (*versus* Li/Li^+) at a constant current of approximately 30 mA g^{-1} up to 50 cycles. Fig. 5(b) presents the

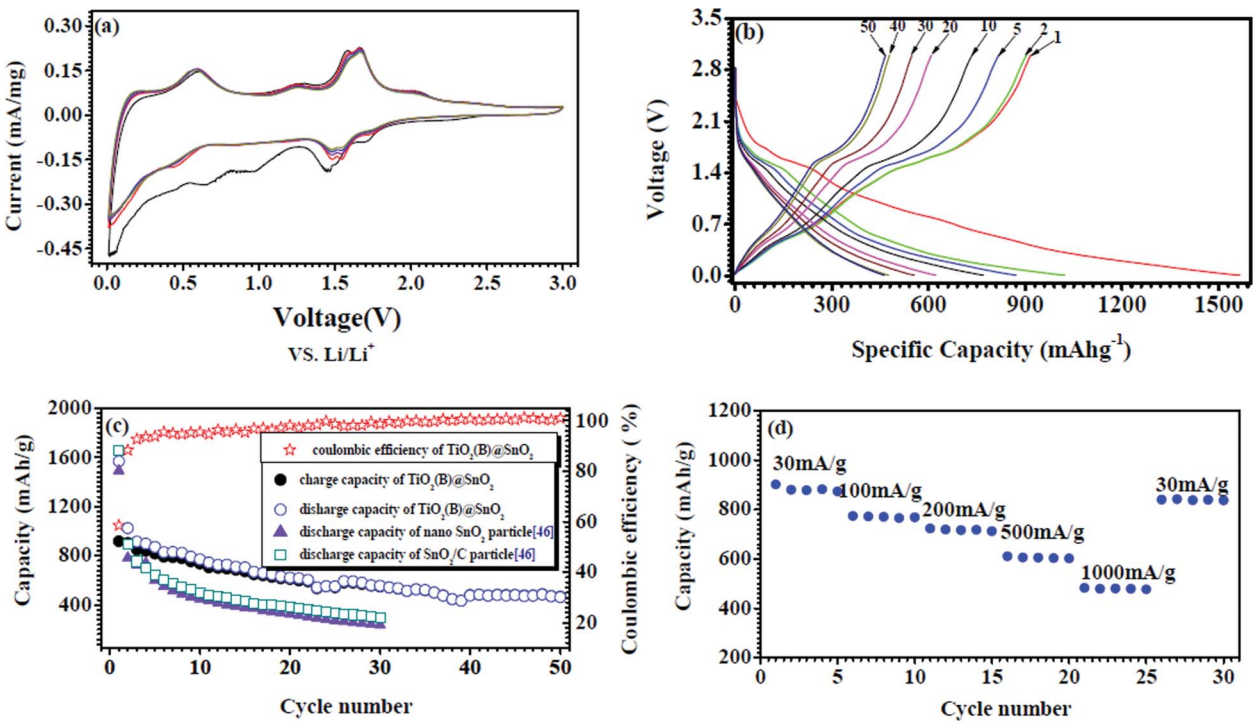

Fig. 5 Electrochemical performance of TiO_2(B)@SnO_2 nanowire electrode cycled between 0.01 and 3.0 V *vs.* Li^+/Li: (a) cyclic voltammograms of TiO_2(B)@SnO_2 nanowire electrode from the first cycle to the fifth cycle at a scan rate of 0.1 mV s^{-1} in the voltage range 0.01–3.0 V. (b) Voltage profiles of TiO_2(B)@SnO_2 nanowire composite electrode at the current density of 30 mA g^{-1} for selected cycles. (c) Capacity–cycle number curves and coulombic efficiency from the first cycle to the 50th cycle of TiO_2(B)@SnO_2 nanowires at the current density of 30 mA g^{-1}, compared with SnO_2 nanoparticle and SnO_2/C nanoparticle electrodes cycled in the same voltage range 0.01–3 V.[47] (d) Charge–discharge capacity of TiO_2@SnO_2 nanowire electrode as a function of the charge–discharge rate (30 mA g^{-1}, 100 mA g^{-1}, 200 mA g^{-1}, 500 mA g^{-1}, 1000 mA g^{-1}).

voltage profiles of a TiO_2(B)@SnO_2 hybrid nanowire electrode at a current density of 30 mA g^{-1}. The first discharge and charge steps deliver a specific capacity of 1566.3 and 916.8 mA h g^{-1}, respectively, with an initial coulombic efficiency of 58.5%. The large initial capacity loss of the TiO_2(B)@SnO_2 composite electrode can be partly attributed to the formation of a thick SEI layer on the electrode,[44] the high specific surface area of the porous SnO_2 nanocrystals in the TiO_2(B)@SnO_2 composite, which consume a much greater quantity of irreversible Li^+ to form the SEI layer as compared with common SnO_2 materials, and further, some Li^+ pathway interception by the Li_2O layer formed on the TiO_2(B) core during discharge–charge cycling.[43] Fig. 5(c) displays the capacity–cycle number curves from the first cycle to the 50th cycle of TiO_2(B)@SnO_2 nanowires at a current density of 30 mA g^{-1}. For comparison, the capacity–cycle number curves from the first cycle to the 30th cycle (0.01–3 V) of the SnO_2 nanoparticle and SnO_2/C nanoparticle electrodes prepared by the molten salt method in our laboratory[47] has also been shown in Fig. 5(c). Compared to the SnO_2 and SnO_2/C nanoparticle electrodes, the TiO_2(B)@SnO_2 composite electrode exhibits greatly improved cycling performance and a higher reversible specific capacity of approximately 463 mA h g^{-1} up to 50 cycles, with high coulombic efficiency of nearly 100%. Fig. 5(d) shows the rate capability of the TiO_2(B)@SnO_2 nanowire electrode, which delivers a capacity of about 873 mA h g^{-1} at a current density of 30 mA g^{-1} after 5 cycles. This value decreases to 769 mA h g^{-1} at 100 mA g^{-1}, 712 mA h g^{-1} at 200 mA g^{-1}, 602 mA h g^{-1} at 500 mA g^{-1}, 477 mA h g^{-1} at 1000 mA g^{-1}, and finally returns to 837 mA h g^{-1} at 30 mA g^{-1} after 5 cycles, which shows the excellent rate capability of the TiO_2(B)@SnO_2 nanowire electrode.

The good electrochemical performance of the TiO_2(B)@SnO_2 composite electrode may be attributed to the following factors: first, as shown in Scheme S1 (ESI†), the core–shell structure of the TiO_2(B)@SnO_2 nanowire, consisting of a TiO_2(B) crystal core inside a shell of porous SnO_2 nanocrystals, is favorable to lithium ion diffusion during charge–discharge cycling, owing to the open continuous channel in the TiO_2(B) core along its axis. Second, the porous amorphous or nanocrystalline SnO_2 particles with their relatively higher specific surface area compared to micron-sized particles ensure electrode–electrolyte contact during discharge–charge cycling and make the greatest contribution to lithium storage capacity, owing to the lower capacity of the hybrid nanowire electrode when cycled beyond 50 cycles between 1.0 and 3.0 V *vs.* Li^+/Li, as shown in Fig. S3,† which is mainly attributable to the TiO_2(B) in the hybrid nanowire. Additionally, the TiO_2(B) core in the composite, to some extent, acts as an effective mechanical support to alleviate the stress aroused during lithium intercalation–de-intercalation, which may play a critical role in the excellent lithium storage capacity and cyclability of the electrode. Finally, the mesopores formed by 3D microstructures (bundles of nanowires) also contribute to the improved electrochemical performance of the electrode, possibly because they facilitate the electrolyte or lithium ion diffusion during charge–discharge processes.

Conclusions

In summary, TiO_2(B)@SnO_2 hybrid nanowires consisting of a TiO_2(B) crystal core inside a shell of porous SnO_2 nanocrystals have been fabricated by a facile hydrothermal process and subsequent liquid phase reaction. This particular architecture of TiO_2(B)@SnO_2 hybrid nanowires has an open continuous channel along the nanowire axis, facilitating lithium ion diffusion, as well as providing effective mechanical support of the TiO_2(B) core, alleviating the stress caused during discharge–charge cycling, and further preventing the pulverization of the Sn nanoparticles. Therefore, this composite delivers a high reversible capacity of ~463 mA h g^{-1} after 50 cycles at a current density of 30 mA g^{-1}, with a high coulombic efficiency of nearly 100%. It also delivers a reversible discharge capacity as high as 477 mA h g^{-1}, when cycled at a current density of 1000 mA g^{-1}. Thus, this composite is a promising potential anode material for lithium-ion batteries, even though the composition and structure of these materials require further improvement by optimizing the fabrication processes of the composite.

Acknowledgements

Part of this work was funded by an Australian Research Council (ARC) Discovery Grant (DP1094261), the Postdoctoral Foundation Program of Fuzhou University (BSH-0601), the Natural Science Foundation Program of Fujian Province (2010J01332, A0510011), the Initial Foundation Program of the Ministry of Education for Returned Exchange Personnel (LXKQ201101), and the Talent Foundation Program of Fuzhou University. The authors also would like to thank Dr Tania Silver at the University of Wollongong for critical reading of the manuscript and Mr. Attard Darren for his great contribution.

References

1 Qin Kuang, Changshi Lao, Zhong Lin Wang, Zhaoxiong Xie and Lansun Zheng, High-Sensitivity Humidity Sensor Based on a Single SnO_2 Nanowire, *J. Am. Chem. Soc.*, 2007, **129**, 6070–6071.
2 V. Sysoev Victor, Joachim Goschnick, Thomas Schneider, Evghenii Strelcov and Andrei Kolmakov, A Gradient Microarray Electronic Nose Based on Percolating SnO_2 Nanowire Sensing Elements, *Nano Lett.*, 2007, **7**(10), 3182–3188.
3 Maojun Zheng, Guanghai Li, Xinyi Zhang, Shiyong Huang, Yong Lei and Lide Zhang, Fabrication and Structural Characterization of Large-Scale Uniform SnO_2 Nanowire Array Embedded in Anodic Alumina Membrane, *Chem. Mater.*, 2001, **13**, 3859–3861.
4 F. Hernández-Ramírez, A. Tarancón, O. Casals, J. Arbiol, A. Romano-Rodríguez and J. R. Morante, High response and stability in CO and humidity measures using a single SnO_2 nanowire, *Sens. Actuators, B*, 2007, **121**, 3–17.
5 Young-Jin Choi, In-Sung Hwang, Jae-Gwan Park, Kyoung Jin Choi, Jae-Hwan Park and Jong-Heun Lee, Novel fabrication of an SnO_2 nanowire gas sensor with high sensitivity, *Nanotechnology*, 2008, **19**, 095508.
6 Fang Song, Huilan Su, Jie Han, Di Zhang and Zhixin Chen, Fabrication and good ethanol sensing of biomorphic SnO_2 with architecture hierarchy of butterfly wings, *Nanotechnology*, 2009, **20**, 495502.
7 Shashwati Sena, Prajakta Kanitkar, Ankit Sharma, K. P. Muthe, Ashutosh Rath, S. K. Deshpande, Manmeet Kaur, R. C. Aiyer, S. K. Gupta and J. V. Yakhmi, Growth of SnO_2/$W_{18}O_{49}$ nanowire hierarchical heterostructure and their application as chemical sensor, *Sens. Actuators, B*, 2010, **147**, 453–460.
8 Muhammad Shahid, Imran Shakir, Seok-Jo Yang and Dae Joon Kang, Facile synthesis of core-shell SnO_2/V_2O_5 nanowires and their efficient photocatalytic property, *Mater. Chem. Phys.*, 2010, **124**, 619–622.
9 Min-Sik Park, Guo-Xiu Wang, Yong-Mook Kang, David Wexler, Shi-Xue Dou and Hua-Kun Liu, Preparation and Electrochemical

Properties of SnO_2 Nanowires for Application in Lithium-Ion Batteries, *Angew. Chem., Int. Ed.*, 2007, **46**, 750–753.
10 Hyesun Kim and Jaephil Cho, Hard templating synthesis of mesoporous and nanowire SnO_2 lithium battery anode materials, *J. Mater. Chem.*, 2008, **18**, 771–775.
11 Z. P. Guo, G. D. Du, Y. Nuli, M. Hossan and H. K. Liu, Ultrafine Porous SnO_2 nanopowders prepared via molten salt process: A highly efficient anode material for lithium-ion batteries, *J. Mater. Chem.*, 2009, **19**, 3253–3257.
12 Lionel Vayssieres and Michael Graetzel, Highly Ordered SnO_2 Nanorod Arrays from Controlled Aqueous Growth, *Angew. Chem., Int. Ed.*, 2004, **43**, 3666–3670.
13 Dong-Feng Zhang, Ling-Dong Sun, Chun-Jiang Jia, Zheng-Guang Yan, Li-Ping You and Chun-Hua Yan, Hierarchical Assembly of SnO_2 Nanorod Arrays on α-Fe_2O_3 Nanotubes: A Case of Interfacial Lattice Compatibility, *J. Am. Chem. Soc.*, 2005, **127**, 13492–13493.
14 Y. C. Lee, Hui Huang, O. K. Tan and M. S. Tse, Semiconductor gas sensor based on Pd-doped SnO_2 nanorod thin films, *Sens. Actuators, B*, 2008, **132**, 239–242.
15 Yi Cheng and P. Xiong, Mechanism and Optimization of pH Sensing Using SnO2 Nanobelt Field Effect Transistors, *Nano Lett.*, 2008, **8**(2), 4179–4184.
16 Y. J. Chen, Q. H. Li, Y. X. Liang, T. H. Wang, Q. Zhao and D. P. Yu, Field-emission from long SnO_2 nanobelt arrays, *Appl. Phys. Lett.*, 2004, **85**(23), 5682–5684.
17 Le Viet Thong, Nguyen Duc Hoa, Dang Thi Thanh Le, Do Thanh Viet, Phuong Dinh Tam, Anh-Tuan Le and Nguyen Van Hieu, On-chip fabrication of SnO_2-nanowire gas sensor: The effect of growth time on sensor performance, *Sens. Actuators, B*, 2010, **146**(1), 361–367.
18 Yong Wang, Hua Chun Zeng and Jim Yang Lee, Highly Reversible Lithium Storage in Porous SnO_2 Nanotubes with Coaxially Grown Carbon Nanotube Overlayers, *Adv. Mater.*, 2006, **18**, 645–649.
19 Wei Zhu, Wenzhong Wang, Haolan Xu and Jianlin Shi, Fabrication of ordered SnO_2 nanotube arrays via a template route, *Mater. Chem. Phys.*, 2006, **99**, 127–130.
20 B. Wang, L. F. Zhu, Y. H. Yang, N. S. Xu and G. W. Yang, Fabrication of a SnO_2 Nanowire Gas Sensor and Sensor Performance for Hydrogen, *J. Phys. Chem. C*, 2008, **112**, 6643–6647.
21 Hao Ming Chen and Ru-Shi Liu, Architecture of Metallic Nanostructures: Synthesis Strategy and Specific Applications, *J. Phys. Chem. C*, 2011, **115**(9), 3513–3527.
22 Yong Wang, Jim Yang Lee and Hua Chun Zeng, Polycrystalline SnO_2 Nanotubes Prepared *via* Infiltration Casting of Nanocrystallites and their Electrochemical Application, *Chem. Mater.*, 2005, **17**, 3899–3903.
23 Yoshio Idota, Tadahiko Kubota, Akihiro Matsufuji, Yukio Maekawa and Tsutomu Miyasaka, Tin-Based Amorphous Oxide: A High-Capacity Lithium-Ion–Storage Material, *Science*, 1997, **276**, 1395–1397.
24 J. L. Tirado, R. Santamaría, G. F. Ortiz, R. Menéndez, P. Lavela, J. M. Jiménez-Mateos, F. J. Gómez García, A. Concheso and R. Alcántara, Tin–carbon composites as anodic material in Li-ion batteries obtained by co-pyrolysis of petroleum vacuum residue and SnO_2 , *Carbon*, 2007, **45**, 1396–1409.
25 Yan Yu, Lin Gu, Chunlei Wang, Abirami Dhanabalan, A. van Aken Peter and Joachim Maier, Encapsulation of Sn@carbon Nanoparticles in Bamboo-like Hollow Carbon Nanofibers as an Anode Material in Lithium-Based Batteries, *Angew. Chem., Int. Ed.*, 2009, **48**, 6485–6489.
26 Jun Liu, Wen Li and Arumugam Manthiram, Dense core–shell structured SnO_2/C composites as high performance anodes for lithium ion batteries, *Chemical Communications*, 2010, **46**, 1437–1439.
27 G. D. Du, C. Zhong, P. Zhang, Z. P. Guo, Z. X. Chen and H. K. Liu, Tin dioxide/carbon nanotube composites with high uniform SnO2 loading as anode materials for lithium ion batteries, *Electrochim. Acta*, 2010, **55**, 2582–2586.
28 H. S. Kim and H. W. Kim, Fabrication and Raman Studies of MgO/SnO_2 Core–Shell Heteronanowires, *Acta Physica Polonica A*, 2009, **116**, 58–61.
29 Z. W. Zhao, Z. P. Guo, D. Wexler, Z. F. Ma, X. Wu and H. K. Liu, Titania nanotube supported Tin anodes for Lithium intercalation, *Electrochem. Commun.*, 2007, **9**, 697–702.
30 Markéta Zukalová, Martin Kalbáč, Ladislav Kavan, Ivan Exnar and Michael Graetzel, Pseudocapacitive Lithium Storage in TiO_2(B), *Chem. Mater.*, 2005, **17**, 1248–1255.
31 Dongjiang Yang, Hongwei Liu, Zhanfeng Zheng, Yong Yuan, Jin-Cai Zhao, R. Waclawik Eric, Xuebin Ke and Huaiyong Zhu, An Efficient Photocatalyst Structure: TiO_2(B) Nanofibers with a Shell of Anatase Nanocrystals, *J. Am. Chem. Soc.*, 2009, **131**, 17885–17893.
32 Wei Li, Chang Liu, Yaxin Zhou, Yang Bai, Xin Feng, Zhuhong Yang, Linghong Lu, Xiaohua Lu and Kwong-Yu Chan, Enhanced Photocatalytic Activity in Anatase/TiO_2(B) Core-Shell Nanofiber, *J. Phys. Chem. C*, 2008, **112**, 20539–20545.
33 Thomas Beuvier, Mireille Richard-Plouet and Luc Brohan, Accurate Methods for Quantifying the Relative Ratio of Anatase and TiO_2(B) Nanoparticles, *J. Phys. Chem. C*, 2009, **113**, 13703–13706.
34 Yang Bai, Wei Li, Chang Liu, Zhuhong Yang, Xin Feng, Xiaohua Lu and Kwong-Yu Chan, Stability of Pt nanoparticles and enhanced photocatalytic performance in mesoporous Pt-(anatase/TiO_2(B)) nanoarchitecture, *J. Mater. Chem.*, 2009, **19**, 7055–7061.
35 G. H. Du, Q. Chen, R. C. Che, Z. Y. Yuan and L. M. Peng, Preparation and structure analysis of titanium oxide nanotubes, *Appl. Phys. Lett.*, 2001, **79**(22), 3702–3704.
36 Q. Chen, G. H. Du, S. Zhang and L. M. Peng, The structure of trititanate nanotubes, *Acta Crystallogr., Sect. B: Struct. Sci.*, 2002, **58**, 587–593.
37 Naofumi Ohtsu, Naoya Masahashi, Yoshiteru Mizukoshi and Kazuaki Wagatsuma, Hydrocarbon Decomposition on a Hydrophilic TiO_2 Surface by UV Irradiation: Spectral and Quantitative Analysis Using in situ XPS Technique, *Langmuir*, 2009, **25**(19), 11586–11591.
38 S. Ben Amor, G. Baud, M. Benmalek, H. Dunlop, R. Frier and M. Jacquet, Titania Coatings on Polyethylene Terephthalate: Adhesion and XPS Studies, *J. Adhes.*, 1998, **65**, 307–329.
39 Min-Sik Park, Yong-Mook Kang, Jung-Ho Kima, Guo-Xiu Wang, Shi-Xue Dou and Hua-Kun Liu, Effects of low-temperature carbon encapsulation on the electrochemical performance of SnO_2 nanopowders, *Carbon*, 2008, **46**, 35–40.
40 Yude Wang, Igor Djerdj, Bernd Smarsly and Markus Antonietti, Antimony-Doped SnO_2 Nanopowders with High Crystallinity for Lithium-Ion Battery Electrode, *Chem. Mater.*, 2009, **21**, 3202–3209.
41 N. Sharma, J. Plévert, Subba Rao, B. V. R. Chowdari and T. J. White, Tin Oxides with Hollandite Structure as Anodes for Lithium Ion Batteries, *Chem. Mater.*, 2005, **17**, 4700–4710.
42 XPS database on Web: http://www.lasurface.com/database/elementxps.php accessed July 2011.
43 Da Deng, Min Gyu Kim, Jim Yang Lee and Jaephil Cho, Green energy storage materials: Nanostructured TiO_2 and Sn-based anodes for lithium-ion batteries, *Energy Environ. Sci.*, 2009, **2**, 818–837.
44 Xiong Wen Lou, Chang Ming Li and A. Archer Lynden, Designed Synthesis of Coaxial SnO_2@carbon Hollow Nanospheres for Highly Reversible Lithium Storage, *Adv. Mater.*, 2009, **21**, 2536–2539.
45 Ladislav Kavan, Martin Kalbáč, Markéta Zukalová, Ivan Exnar, Volker Lorenzen, Reinhard Nesper and Michael Graetzel, Lithium Storage in Nanostructured TiO_2 Made by Hydrothermal Growth, *Chem. Mater.*, 2004, **16**, 477–485.
46 Jinwei Xu, Caihong Jia, Bin Cao and W. F. Zhang, Electrochemical properties of anatase TiO_2 nanotubes as an anode material for lithium-ion batteries, *Electrochim. Acta*, 2007, **52**, 8044–8047.
47 Bin Liu, Zai Ping Guo, Guodong Du, Yanna Nulid, Mohd Faiz Hassan and Dianzeng Jia, In situ synthesis of ultra-fine, porous, tin oxide-carbon nanocomposites *via* a molten salt method for lithium-ion batteries, *J. Power Sources*, 2010, **195**, 5382–5386.

